

1 STUDY SITE

1 The Guttannen (GT) site in the Bern region lies at 1047 m a.s.l.. In the winter (Oct-Apr), mean daily
 2 minimum and maximum air temperatures vary between -13 and 15 °C. Clear skies are rare, averaging
 3 around 7 days during winter (Meteoblue, 2020). The site was situated adjacent to a stream resulting in high
 4 humidity values across the study period. An automatic weather station (AWS) was adjacent to the wooden
 5 boundary as shown in Fig. ???. The fountain used for spraying water had a height of 1.35 m, and was placed
 6 in the centre of the wooden enclosure. The water was transferred from a spring water source and flowed via
 7 a flowmeter and an air escape valve to the nozzle. The air escape valve was installed to avoid errors in the
 8 flow measurements due to air bubbles. In addition, a webcam guaranteed a continuous survey of the site
 9 during the construction of the Icestupa.

10 1.1 Measurements and Data

11 Measurements comprising air temperature, relative humidity, water flow rate, wind speed and direction
 12 were made every 5 minutes throughout the construction period. The water flow rate or discharge was
 13 measured via an ultrasonic sensor attached to the fountain supply pipeline.

14 In addition, we used ERA5 reanalysis dataset (Copernicus Climate Change Service (C3S), 2017) for
 15 filling data gaps and adding data that were not measured directly at the EP site. The 2 m temperature
 16 parameter correlated with air temperature ($r^2 = 0.9$), surface pressure parameter correlated with air
 17 pressure ($r^2 = 1$) and 10m wind speed parameter (derived from horizontal and vertical components)
 18 correlated with wind speed ($r^2 = 0.6$). The ERA5 reanalysis dataset has a good correlation with lower
 19 elevation sites in Switzerland (Scherrer, 2020). The hourly ERA5 data and the 10 minute Plaffeien AWS
 20 data were linearly interpolated to the 5 minute data frequency of the EP AWS.

21 The ERA5 grid point chosen (Latitude 46° 38' 24" N, Longitude 7° 14' 24" E) for the EP site was around
 22 9 km away from the actual site. All the ERA5 variables were therefore fitted with the EP dataset via linear
 23 regressions.

24 1.1.1 Drone Measurements for calibration and validation

25 Several Drone flights were conducted in every AIR site. The DEM generated through these flights were
 26 analysed to obtain the circumference and volume of the ice structure. The mean circumference measured
 27 during the fountain duration was set as the spray radius (r_{spray}) for model initialisation.

Team	Location	Code	Fountain duration	Drone flights	r_{spray}
Icestupa Competition	Gangles, India	IC21	Jan 18 - Mar 10, 2021	6	10.8m
Guttannen Bewegt	Guttannen, Switzerland	GB21	Nov 22 - Feb 21, 2021	9	6.9 m
Guttannen Bewegt	Guttannen, Switzerland	GB20	Jan 3 - Feb 27, 2020	3	7.7 m
Eispalast	Schwarzsee, Switzerland	EP19	Jan 30 - Feb 16, 2019	0	1.2 m

2 MODEL SETUP

30 A bulk energy and mass balance model is used to calculate the amounts of ice, meltwater, water vapour
 31 and runoff water of the AIR every hour. This model consists of four modules which estimates the AIR, a)
 32 geometric evolution , b) energy balance, c) surface temperature and d) mass balance.

33 2.1 Geometric evolution

34 Radius r_{ice}^i and height h_{ice}^i define the dimensions of the AIR assuming its geometry to be a cone. The
 35 surface area A^i exposed to the atmosphere and volume V^i are:

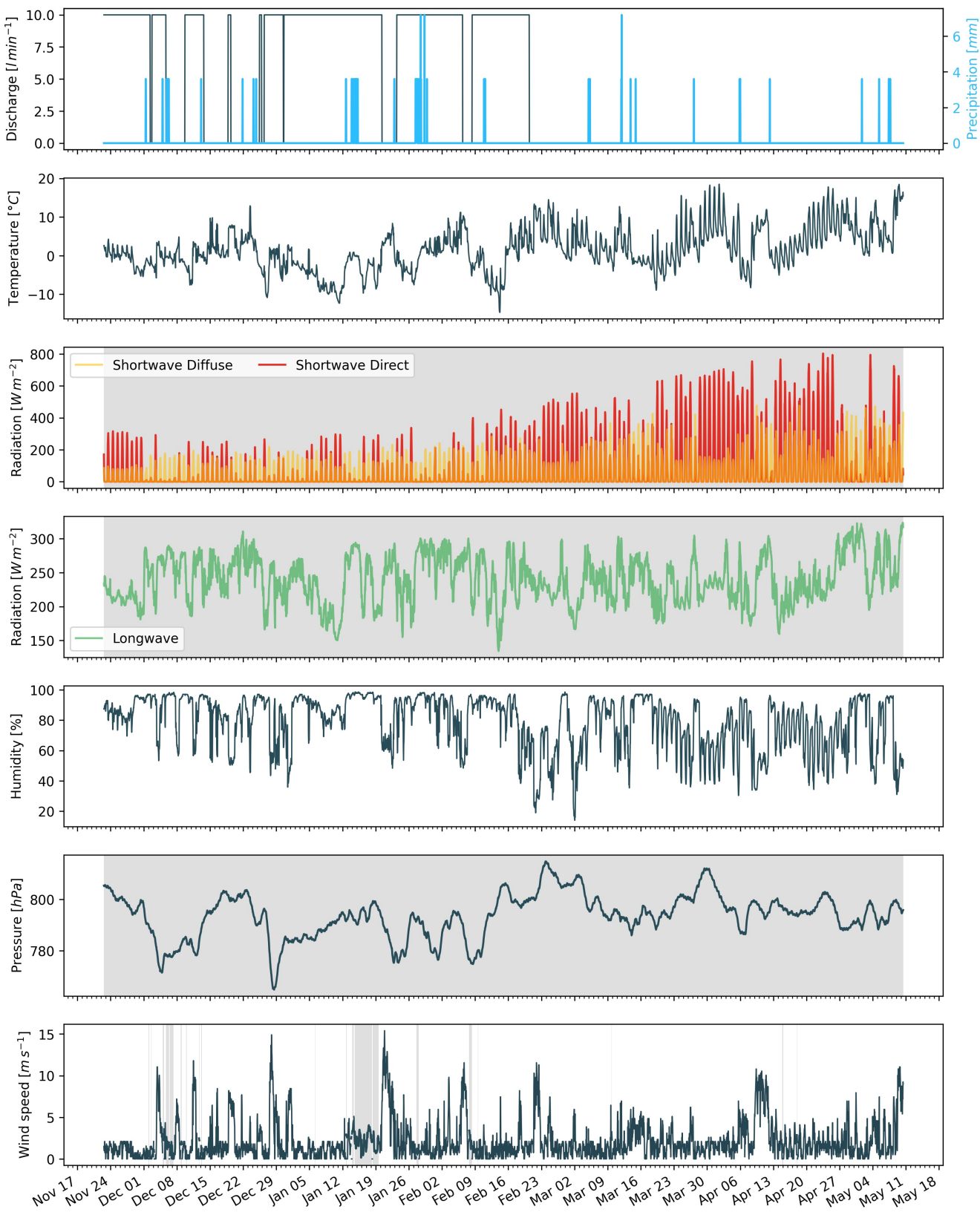


Figure 1. Measurements at the AWS of GB21 were used as main model input data in hourly frequency. Missing data, data gaps and errors were filled from the ERA5 dataset (shaded regions).

$$A = \pi \cdot r_{ice} \cdot \sqrt{r_{ice}^2 + h_{ice}^2} \quad (1)$$

$$V = \pi/3 \cdot r_{ice}^2 \cdot h_{ice} \quad (2)$$

36 Note that we do not specify the time step superscript i of the shape variables A , V , r_{ice} and h_{ice} for
 37 brevity. The equations used henceforth display model time step superscript i only if it is different from the
 38 current time step.

39 With the mass of the AIR M_{ice} , its current volume can also be expressed as:

$$V = M_{ice}/\rho_{ice} \quad (3)$$

40 where ρ_{ice} is the density of ice (917 kg m^{-3}).

41 The influence of the AIR fountain is parameterised by the fountain water temperature T_w and its spray
 42 radius r_{spray} . The initial radius r_0 of the AIR is assumed to be r_{spray} . The initial height h_0 depends on the
 43 dome volume V_{dome} used to construct the AIR as follows:

$$h_0 = \Delta x + \frac{3 \cdot V_{dome}}{\pi r_{spray}^2} \quad (4)$$

44 where Δx is the surface layer thickness (defined in Section 2.2)

45 During subsequent time steps, the dimensions of the AIR evolve assuming a uniform ice formation and
 46 decay across its surface area with an invariant slope $s_{cone} = \frac{h_{ice}}{r_{ice}}$. During these time steps, the volume is
 47 parameterised using Eqn. 2 as:

$$V = \frac{\pi \cdot r_{ice}^3 \cdot s_{cone}}{3} \quad (5)$$

48 However, the Icestupa cannot outgrow the maximum range of the water droplets ($(r_{ice})_{max} = r_F$).
 49 Combining equations 2, 4, 3 and 5, the geometric evolution of the Icestupa at each time step i can be
 50 determined by considering the following rules:

$$(r_{ice}, h_{ice}) = \begin{cases} (r_{spray}, h_0) & \text{if } i = 0 \\ (r_{ice}^{i-1}, \frac{3 \cdot M_{ice}}{\pi \cdot \rho_{ice} \cdot (r_{ice}^{i-1})^2}) & \text{if } r_{ice}^{i-1} \geq r_F \text{ and } \Delta M_{ice} > 0 \\ (\frac{3 \cdot M_{ice}}{\pi \cdot \rho_{ice} \cdot s_{cone}})^{1/3} \cdot (1, s_{cone}) & \text{otherwise} \end{cases} \quad (6)$$

51 where $\Delta M_{ice} = M_{ice}^{i-1} - M_{ice}^{i-2}$

52 2.2 Energy Balance

53 The energy balance equation (Hock, 2005) for the AIR is formulated as follows:

$$q_{SW} + q_{LW} + q_L + q_S + q_F + q_G = q_{surf} \quad (7)$$

54 where q_{surf} is the surface energy flux in [$W\ m^{-2}$]; q_{SW} is the net shortwave radiation; q_{LW} is the net
 55 longwave radiation; q_L and q_S are the turbulent latent and sensible heat fluxes. q_F represents the heat
 56 exchange of the fountain water droplets with the AIR ice surface. q_G represents ground heat flux between
 57 Icestupa surface and Icestupa interior. Energy transferred in the direction of the ice surface is always
 58 denoted as positive and away as negative.

59 Equation 7 is usually referred to as the energy budget for “the surface”, but practically it must apply
 60 to a surface layer of ice with a finite thickness Δx . The energy flux acts upon the Icestupa surface layer
 61 which has an upper and a lower boundary defined by the atmosphere and the ice body of the Icestupa,
 62 respectively. The parameter selection for Δx is based on the following two arguments: (a) the ice thickness
 63 Δx should be small enough to represent the surface temperature variations every model time step Δt and
 64 (b) Δx should be large enough for these temperature variations to not reach the bottom of the surface layer.
 65 Therefore, we introduced a 20 mm thick surface layer for a model time step of 1 hour, over which the
 66 energy balance is calculated. A sensitivity analysis was later performed to understand the influence of this
 67 factor. Here, we define the surface temperature T_{ice} to be the modelled average temperature of the Icestupa
 68 surface layer and the energy flux q_{surf} is assumed to act uniformly across the Icestupa area A .

69 2.2.1 Net Shortwave Radiation q_{SW}

70 The net shortwave radiation q_{SW} is computed as follows:

$$71 \quad q_{SW} = (1 - \alpha) \cdot (SW_{direct} \cdot f_{cone} + SW_{diffuse}) \quad (8)$$

72 where SW_{direct} and $SW_{diffuse}$ are the ERA5 direct and diffuse short wave radiation, α is the modelled
 73 albedo and f_{cone} is the area fraction of the ice structure exposed to the direct shortwave radiation.

74 We model the albedo using a scheme described in Oerlemans and Knap (1998). The scheme records the
 75 decay of albedo with time after fresh snow is deposited on the surface. δt records the number of time steps
 after the last snowfall event. After snowfall, albedo changes over a time step, δt , as

$$76 \quad \alpha = \alpha_{ice} + (\alpha_{snow} - \alpha_{ice}) \cdot e^{(-\delta t)/\tau} \quad (9)$$

77 where α_{ice} is the bare ice albedo value (0.35), α_{snow} is the snow ice albedo value (0.85) and τ is a decay
 78 rate, which determines how fast the albedo of the ageing snow reaches this value. The decay rate τ is
 79 assumed to have a base value of 10 days similar to values obtained by Schmidt et al. (2017) for wet surfaces
 80 and its maximal value is set based on observations by Oerlemans and Knap (1998) as shown in Table 1.
 81 Furthermore, the albedo α varies depending on the water source that formed the current Icestupa surface.
 82 Correspondingly, the albedo is reset to the value of bare ice albedo if the fountain is spraying water onto
 83 the current ice surface and to the value of fresh snow albedo if a snowfall event occurred. Snowfall events
 84 are assumed if the air temperature is below $T_{ppt} = 1^{\circ}C$ (Fujita and Ageta, 2000).

85 The area fraction f_{cone} of the ice structure exposed to the direct shortwave radiation depends on the
 86 shape considered. The direct solar radiation incident on the AIR surface is first decomposed into horizontal
 87 and vertical components using the solar elevation angle θ_{sun} . For a conical shape, half of the total curved
 88 surface is exposed to the vertical component of the direct shortwave radiation and the projected triangle
 89 of the curved surface is exposed to the horizontal component of the direct shortwave radiation. The solar
 90 elevation angle θ_{sun} used is modelled using the parametrisation proposed by Woolf (1968). Accordingly,
 f_{cone} is determined as follows:

$$f_{cone} = \frac{(0.5 \cdot r_{ice} \cdot h_{ice}) \cdot \cos\theta_{sun} + (\pi \cdot r_{ice}^2 / 2) \cdot \sin\theta_{sun}}{\pi \cdot r_{ice} \cdot (r_{ice}^2 + h_{ice}^2)^{1/2}} \quad (10)$$

91 The ERA5 diffuse shortwave radiation is assumed to impact the conical Icestupa surface uniformly.

92 2.2.2 Net Longwave Radiation q_{LW}

93 The net longwave radiation q_{LW} is determined as follows:

$$q_{LW} = LW_{in} - \sigma \cdot \epsilon_{ice} \cdot (T_{ice} + 273.15)^4 \quad (11)$$

94 where T_a represents the measured air temperature, T_{ice} is the modelled surface temperature, both
 95 temperatures are given in $^{\circ}\text{C}$, $\sigma = 5.67 \cdot 10^{-8} \text{ J m}^{-2} \text{ s}^{-1} \text{ K}^{-4}$ is the Stefan-Boltzmann constant, LW_{in}
 96 denotes the incoming longwave radiation derived from the ERA5 dataset and ϵ_{ice} is the corresponding
 97 emissivity value for the Icestupa surface (see Table 1).

98 2.2.3 Turbulent sensible q_S and latent q_L heat fluxes

99 The turbulent sensible q_S and latent heat q_L fluxes are computed with the following expressions proposed
 100 by Garratt (1992):

$$q_S = c_a \cdot \rho_a \cdot p_a / p_{0,a} \cdot \frac{\kappa^2 \cdot v_a \cdot (T_a - T_{ice})}{(\ln \frac{h_{AWS}}{z_{ice}})^2} \quad (12)$$

$$q_L = 0.623 \cdot L_s \cdot \rho_a / p_{0,a} \cdot \frac{\kappa^2 \cdot v_a (p_{v,a} - p_{v,ice})}{(\ln \frac{h_{AWS}}{z_{ice}})^2} \quad (13)$$

101 where h_{AWS} is the measurement height above the ground surface of the AWS (in m), v_a is the wind
 102 speed in $[m s^{-1}]$, c_a is the specific heat of air at constant pressure ($1010 \text{ J kg}^{-1} \text{ K}^{-1}$), ρ_a is the air density
 103 at standard sea level (1.29 kg m^{-3}), $p_{0,a}$ is the air pressure at standard sea level (1013 hPa), κ is the
 104 von Karman constant (0.4), L_s is the heat of sublimation (2848 kJ kg^{-1}) and z_{ice} (1.7 mm) denotes the
 105 roughness length of ice (momentum and scalar). The vapor pressures over air ($p_{v,a}$) and ice ($p_{v,ice}$) was
 106 obtained using the following formulation given in WMO (2018):

$$p_{v,a} = 6.107 \cdot 10^{(7.5 \cdot T_a / (T_a + 237.3))} \\ p_{v,ice} = (1.0016 + 3.15 \cdot 10^{-6} \cdot p_a - 0.074 \cdot p_a^{-1}) \cdot (6.112 \cdot e^{(22.46 \cdot T_{ice} / (T_{ice} + 272.62))}) \quad (14)$$

107 where p_a is the measured air pressure in [hPa].

108 2.2.4 Fountain water heat flux q_F

109 The interaction between the fountain water and the ice surface is taken into account by assuming that
 110 the ice surface temperature remains constant at 0°C during time steps when the fountain is active. This
 111 process can be divided into two simultaneous steps: (a) the water temperature T_{water} is cooled to 0°C
 112 and (b) the ice surface temperature is warmed to 0°C . Process (a) transfers the necessary energy for
 113 process (b) throughout the fountain runtime. We further assume that this process is instantaneous, i.e. the

114 ice temperature is immediately set to 0°C within just one time step Δt when the fountain is switched on.
 115 Thus, the heat flux caused by the fountain water is calculated as follows:

$$q_F = \begin{cases} 0 & \text{if } \Delta M_F = 0 \\ \frac{\Delta M_F \cdot c_{water} \cdot T_{water}}{\Delta t \cdot A} + \frac{\rho_{ice} \cdot \Delta x \cdot c_{ice} \cdot T_{ice}}{\Delta t} & \text{if } \Delta M_F > 0 \end{cases} \quad (15)$$

116 with c_{ice} as the specific heat of ice.

117 2.2.5 Bulk Icestupa heat flux q_G

118 The bulk Icestupa heat flux q_G corresponds to the ground heat flux in normal soils and is caused by the
 119 temperature gradient between the surface layer (T_{ice}) and the ice body (T_{bulk}). It is expressed by using the
 120 heat conduction equation as follows:

$$q_G = k_{ice} \cdot (T_{bulk} - T_{ice}) / l_{ice} \quad (16)$$

121 where k_{ice} is the thermal conductivity of ice ($2.123 \text{ W m}^{-1} \text{ K}^{-1}$), T_{bulk} is the mean temperature of the
 122 ice body within the Icestupa and l_{ice} is the average distance of any point in the surface to any other point in
 123 the ice body. T_{bulk} is initialised as 0°C and later determined from Eqn. 16 as follows:

$$T_{bulk}^{i+1} = T_{bulk} - (q_G \cdot A \cdot \Delta t) / (M_{ice} \cdot c_{ice}) \quad (17)$$

124 Since AIR's typically have conical shapes with $r_{ice} \gg h_{ice}$, we assume that the center of mass of the ice
 125 body is near the base of the fountain. Thus, the distance of every point in the AIR surface layer from the ice
 126 body's center of mass is between h_{ice} and r_{ice} . So we calculate q_G here assuming $l_{ice} = (r_{ice} + h_{ice})/2$.

127 2.3 Surface temperature

128 The available energy q_{surf} can act on the surface of the AIR to a) change its temperature, b) melt ice or
 129 c) freeze ice. So Eqn. 7 can be rewritten as:

$$q_{surf} = q_{freeze/melt} + q_T \quad (18)$$

130 where q_T , q_{freeze} and q_{melt} represent energy associated with process (a), (b) and (c) respectively.

131 To distribute the surface energy flux into these three components, we categorize the model time steps
 132 as freezing or melting events. Freezing events can only occur if there is fountain water available and the
 133 surface energy flux is negative. But just these two conditions are not sufficient as the latent heat energy
 134 can only contribute to temperature fluctuations. So to prevent latent heat energy from turning a melting
 135 event into a freezing event an additional condition namely $(q_{surf} - q_L) < 0$ is required. Thus, freezing and
 136 melting events are identified as follows:

$$q_{freeze/melt} = \begin{cases} q_{freeze} & \text{if } \Delta M_F > 0 \text{ and } q_{surf} < 0 \text{ and } (q_{surf} - q_L) < 0 \\ q_{melt} & \text{otherwise} \end{cases} \quad (19)$$

137 During a freezing event, the available energy $(q_{surf} - q_L)$ can either be sufficient or insufficient to
 138 freeze the fountain water available. If insufficient, the additional energy further cools down the surface
 139 temperature. So the surface energy flux distribution during a freezing event can be represented as:

Table 1. Free parameters in the model categorised as constant, uncertain and site parameters. Base value (B) and uncertainty (U) were taken from the literature. For assumptions (assum.), the uncertainty was chosen to be relatively large (5 %). For measurements (meas.), the uncertainty due to parallax errors is chosen to be (1 %).

Constant Parameters	Symbol	Value	References
Van Karman constant	κ	0.4	B: Cuffey and Paterson
Stefan Boltzmann constant	σ	$5.67 \cdot 10^{-8} W m^{-2} K^{-4}$	B: Cuffey and Paterson
Air pressure at sea level	$p_{0,a}$	1013 hPa	B: Mölg and Hardy
Density of water	ρ_w	$1000 kg m^{-3}$	B: Cuffey and Paterson
Density of ice	ρ_{ice}	$917 kg m^{-3}$	B: Cuffey and Paterson
Density of air	ρ_a	$1.29 kg m^{-3}$	B: Mölg and Hardy
Specific heat of ice	c_{ice}	$2097 J kg^{-1} ^\circ C^{-1}$	B: Cuffey and Paterson
Specific heat of water	c_w	$4186 J kg^{-1} ^\circ C^{-1}$	B: Cuffey and Paterson
Specific heat of air	c_a	$1010 J kg^{-1} ^\circ C^{-1}$	B: Mölg and Hardy
Thermal conductivity of ice	k_{ice}	$2.123 W m^{-1} K^{-1}$	B: Bonales et al.
Latent Heat of Sublimation	L_s	$2848 kJ kg^{-1}$	B: Cuffey and Paterson
Latent Heat of Fusion	L_f	$334 kJ kg^{-1}$	B: Cuffey and Paterson
Uncertain Parameters		Range	
Precipitation	T_{ppt}	$1 ^\circ C$	$\pm 1 ^\circ C$
Temperature threshold			B + U: Fujita and Ageta, Zhou et al.
Ice Emissivity	ϵ_{ice}	0.95	[0.949,0.993]
Ice Albedo	α_{ice}	0.35	$\pm 5 \%$
Snow Albedo	α_{snow}	0.85	$\pm 5 \%$
Albedo Decay Rate	τ	10 days	[1, 22] days
Surface layer thickness	Δx	20 mm	[1, 10] mm
Fountain Parameters		Range	
Spray Radius	r_{spray}		$\pm 5 \%$
Water temperature	T_{water}	$1 ^\circ C$	[0, 5] $^\circ C$

$$(q_{freeze}, q_T) = \begin{cases} (q_{surf} - q_L, q_L) & \text{if } \Delta M_F \geq -\frac{(q_{surf} - q_L)A \cdot \Delta t}{L_f} \\ (\frac{\Delta M_F \cdot L_f}{A \cdot \Delta t}, q_{surf} + \frac{\Delta M_F \cdot L_f}{A \cdot \Delta t}) & \text{if } \Delta M_F < -\frac{(q_{surf} - q_L)A \cdot \Delta t}{L_f} \end{cases} \quad (20)$$

140 During a melting event, the surface energy flux (q_{surf}) is first used to change the surface temperature to
 141 T_{temp} calculated as:

$$T_{temp} = \frac{q_{surf} \cdot \Delta t}{\rho_{ice} \cdot c_{ice} \cdot \Delta x} + T_{ice} \quad (21)$$

142 If $T_{temp} > 0^\circ C$, then energy is reallocated from q_T to q_{melt} to maintain surface temperature at melting
 143 point. So the surface energy flux distribution during a melting event can be represented as:

$$(q_{melt}, q_T) = \begin{cases} (0, q_{surf}) & \text{if } T_{temp} < 0 \\ \left(\frac{T_{temp} \cdot \rho_{ice} \cdot c_{ice} \cdot \Delta x}{\Delta t}, q_{surf} - \frac{T_{temp} \cdot \rho_{ice} \cdot c_{ice} \cdot \Delta x}{\Delta t}\right) & \text{if } T_{temp} > 0 \end{cases} \quad (22)$$

144 2.4 Mass Balance

145 The mass balance equation for an AIR is represented as:

$$\frac{\Delta M_F + \Delta M_{ppt} + \Delta M_{dep}}{\Delta t} = \frac{\Delta M_{ice} + \Delta M_{water} + \Delta M_{sub} + \Delta M_{runoff}}{\Delta t} \quad (23)$$

146 where M_F is the discharge of the fountain; M_{ppt} is the cumulative precipitation; M_{dep} is the cumulative
 147 accumulation through water vapour deposition; M_{ice} is the cumulative mass of ice; M_{water} is the cumulative
 148 mass of melt water; M_{sub} represents the cumulative water vapor loss by sublimation and M_{runoff} represents
 149 the fountain discharge runoff that did not interact with the AIR. The LHS of equation 23 represents the rate
 150 of mass input and the RHS represents the rate of mass output for an AIR.

151 Precipitation input is calculated as shown in equation 24a where ρ_w is the density of water (1000
 152 $kg m^{-3}$), ppt is the measured precipitation rate in $[m s^{-1}]$ and T_{ppt} is the temperature threshold below
 153 which precipitation falls as snow. Here, snowfall events were identified using T_{ppt} as $1^{\circ}C$. Snow mass
 154 input is calculated by assuming a uniform deposition over the entire circular footprint of the Icestupa.

155 The latent heat flux is used to estimate either the evaporation and condensation processes or sublimation
 156 and deposition processes as shown in equation 24b. During time steps at which surface temperature is
 157 below $0^{\circ}C$ only sublimation and deposition can occur, but if the surface temperature reaches $0^{\circ}C$,
 158 evaporation and condensation can also occur. As the differentiation between evaporation and sublimation
 159 (and condensation and deposition) when the air temperature reaches $0^{\circ}C$ is challenging, we assume
 160 that negative (positive) latent heat fluxes correspond only to sublimation (deposition), i.e. no evaporation
 161 (condensation) is calculated.

162 Since we have categorized every time step as a freezing and melting event, we can determine the meltwater
 163 and ice generated using the associated energy fluxes as shown in equations 24c and 24d. Having calculated
 164 all the other mass components the fountain wastewater generated every time step can be calculated using
 165 equation 24e.

$$\frac{\Delta M_{ppt}}{\Delta t} = \begin{cases} \pi \cdot r_{ice}^2 \cdot \rho_w \cdot ppt & \text{if } T_a < T_{ppt} \\ 0 & \text{if } T_a \geq T_{ppt} \end{cases} \quad (24a)$$

$$\left(\frac{\Delta M_{dep}}{\Delta t}, \frac{\Delta M_{sub}}{\Delta t}\right) = \begin{cases} \frac{q_L \cdot A}{L_s} \cdot (1, 0) & \text{if } q_L \geq 0 \\ \frac{q_L \cdot A}{L_s} \cdot (0, -1) & \text{if } q_L < 0 \end{cases} \quad (24b)$$

$$\frac{\Delta M_{water}}{\Delta t} = \frac{q_{melt} \cdot A}{L_f} \quad (24c)$$

$$\frac{\Delta M_{ice}}{\Delta t} = \frac{q_{freeze} \cdot A}{L_f} + \frac{\Delta M_{ppt}}{\Delta t} + \frac{\Delta M_{dep}}{\Delta t} - \frac{\Delta M_{sub}}{\Delta t} - \frac{\Delta M_{melt}}{\Delta t} \quad (24d)$$

$$\frac{\Delta M_{runoff}}{\Delta t} = \frac{\Delta M_F - \Delta M_{ice}}{\Delta t} \quad (24e)$$

Table 2. Summary of mass balance components for the EP experiment after the fountain spray was stopped (on 15th February 2019) and at the end of the model run (on 5th April). All parameters except M_F were modelled.

	Mass Component	Model ends
Input	M_F	1,000,041 kg
	M_{ppt}	29,533 kg
	M_{dep}	4,755 kg
Output	M_{water}	196,011 kg
	M_{ice}	12,304 kg
	M_{sub} M_{runoff}	4,747 kg 821,267 kg

166 Considering AIRs as water reservoirs, we can quantify their potential through the amount of water they
 167 store (storage quantity) and the length of time they store it (storage duration). Another means of comparing
 168 different Icestupas is through their water storage efficiency defined accordingly as:

$$\text{Storage Efficiency} = \frac{M_{water}}{(M_F + M_{ppt} + M_{dep})} \cdot 100 \quad (25)$$

3 MODEL RESULTS

Mass	GB21	GB20	EP19	IC21
M_F	1000040.7	778142.0	18203.8	2982600.0
M_{dep}	4754.9	2983.5	24.1	3824.5
M_{ice}	12304.4	30232.2	8.8	511698.5
M_{ppt}	29532.9	9707.1	143.7	0.0
M_{runoff}	821266.5	672174.8	17766.0	2409393.4
M_{sub}	4746.8	4041.8	4.6	36777.3
M_{water}	196010.8	107090.0	621.4	102802.2

170 The model was forced with meteorological data from 30th January to 5th April 2019 (Fig. 1) and various
 171 parameters (see Table 1) to calculate the mass and energy balance of the Icestupa.

3.1 Energy and mass balance calculation

173 Daily averages of some components of the energy balance are shown in Fig. 2 (b). On average during
 174 the experiment duration, the total energy balance was almost zero. Net shortwave radiation (33 W m^{-2}),
 175 sensible (10 W m^{-2}) and latent heat flux (2 W m^{-2}) with a mostly positive flux towards the surface of the
 176 icestupa were compensated by the surf longwave radiation (- 34 W m^{-2}) and the melt energy (- 12 W m^{-2}).
 177 The contributions of other fluxes were negligible in comparison.

178 Net shortwave radiation is the main input to, and the most varying energy flux on the ice surface. Its
 179 variability is controlled by the surface albedo α and the area fraction f_{cone} which therefore represent key
 180 variables in the energy balance (Fig. ?? (b)). Although global radiation flux reached a daily maximum
 181 value of 339 W m^{-2} , q_{SW} only went up to 98 W m^{-2} . This is caused by the fact that only about 30 % of
 182 the direct solar radiation influenced the Icestupa surface as shown by the area fraction f_{cone} in Fig. ?? (a).

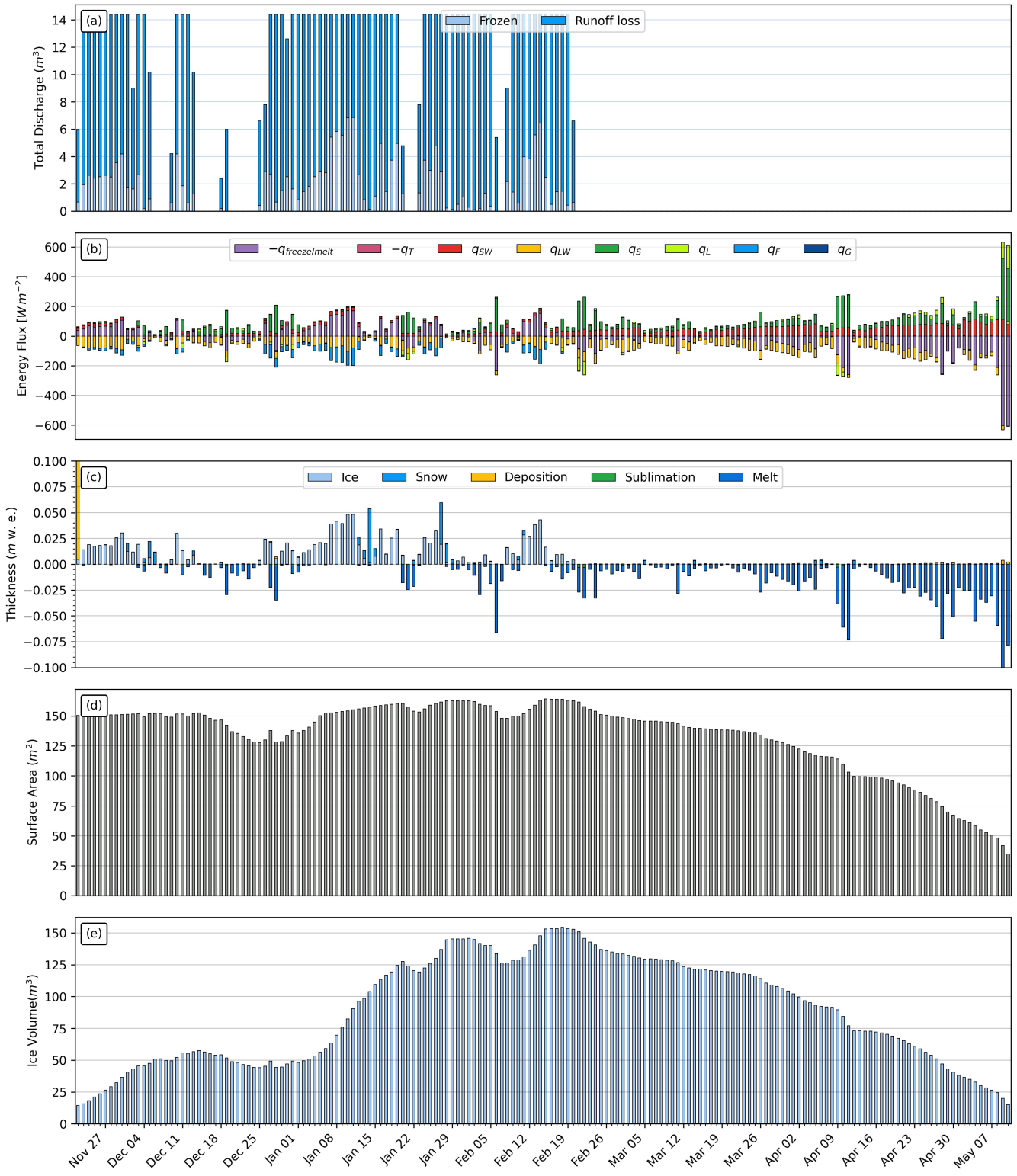


Figure 2. (a) Fountain discharge (b) energy flux components, (c) mass flux components (d) surface area and (e) volume of the Icestupa in daily time steps. q_{SW} is the net shortwave radiation; q_{LW} is the net longwave radiation; q_L and q_S are the turbulent latent and sensible heat fluxes. q_F represents the interactions of the fountain water with the AIR surface layer. q_G quantifies the heat conduction process between the AIR surface layer and the ice body.

183 Snowfall is the atmospheric variable connected most closely and proportionally to albedo. Higher and/or
184 more frequent snowfall thus decreases the energy available for melt due to the corresponding increase in α .

185 q_{LW} was predominantly negative indicating that this energy balance component drove the freezing of
186 the ice structure. Daily values of q_{LW} ranged from -89 to 21 W m^{-2} . Turbulent sensible heat flux q_S
187 contributed mostly to the melt of the ice structure. Daily values of q_S ranged from -14 to 26 W m^{-2} .
188 Deposition/condensation was favored over evaporation/sublimation during 95 % of the model runtime.
189 Daily values of the turbulent latent heat flux q_L ranged from -10 to 15 W m^{-2} . Since the mean of q_L was
190 positive, the Icestupa gained mass cumulatively from the atmosphere due to the condensation process.
191 Fountain water heat flux q_F had a mean of zero as it was only nonzero during 1002 time steps or around
192 100 hours. Daily values of q_F ranged from -1 to 6 W m^{-2} . The contribution of heat flux by conduction
193 q_G was also minimal as it only varied between -6 to 12 W m^{-2} with a mean of 0 W m^{-2} . The energy
194 contributing to surface temperature changes (q_T) was insignificant in comparison to the energy spent on
195 freezing and melting (q_{melt}). The resulting bulk temperature and the surface temperature are shown in Fig.
196 ?? (b). For the total considered period, q_{LW} accounted for 33.8% of overall energy turnover. The energy
197 turnover is calculated as the sum of energy fluxes in absolute values. q_{SW} accounted for 31.3%, followed
198 by q_{melt} (19%), q_S (9.6%), q_L (3.6%), q_G (2.4%), q_F (0.2%) and q_T (0.4%).

199 Fig. 2 (c) represents the mass fluxes associated with these energy exchanges expressed in m w.e. It
200 shows the ice and meltwater formed due to q_{melt} , snow accumulated due to precipitation, water vapour
201 deposition/condensation and sublimation/evaporation due to q_L . Growth rate ($\frac{\Delta M_{ice}}{\Delta t}$) shows a better
202 correlation with surf energy flux ($r^2 = 0.15$) compared to Icestupa surface area ($r^2 = 0.04$). This is
203 because the variance in growth rate is mostly due to the variance in q_{surf} as illustrated in Fig. 2. Since r_{ice}
204 was initialised with the spray radius r_{spray} , the surface area maintains a maximum initially until the energy
205 flux becomes positive. This trend favours the positive over the negative thickness changes resulting in a
206 steep increase and gradual melting of ice volume as can be seen in Fig. ??.

207 The total water used for the Icestupa development includes contributions from the fountain (97.3%),
208 snowfall (2.5 %), condensation (0.2 %) as shown in Table 2. The maximum ice mass during the whole
209 measurement period was 809 kg , which occurred after the last fountain run on Feb 16th 2019 in the morning.
210 Therefore, in the case of EP we used a water input of $18,558 \text{ kg}$, with a resultant storage efficiency of only
211 5.5 %.

REFERENCES

- 212 Bonales, L. J., Rodriguez, A. C., and Sanz, P. D. (2017). Thermal conductivity of ice prepared under
213 different conditions. *International Journal of Food Properties* 20, 610–619. doi:10.1080/10942912.
214 2017.1306551
- 215 [Dataset] Copernicus Climate Change Service (C3S) (2017). Era5: Fifth generation ecmwf atmospheric
216 reanalyses of the global climate. [Available at <https://cds.climate.copernicus.eu/cdsapp#!/home>, accessed 2019-10-01]
- 218 Cuffey, K. M. and Paterson, W. S. B. (2010). *The Physics Of Glaciers* (Elsevier)
- 219 Fujita, K. and Ageta, Y. (2000). Effect of summer accumulation on glacier mass balance on the
220 tibetan plateau revealed by mass-balance model. *Journal of Glaciology* 46, 244–252. doi:10.3189/
221 172756500781832945
- 222 Garratt, J. R. (1992). *The Atmospheric Boundary Layer* (Cambridge University Press)
- 223 Hock, R. (2005). Glacier melt: a review of processes and their modelling. *Progress in Physical Geography:*
224 *Earth and Environment* 29, 362–391

- 225 Hori, M., Aoki, T., Tanikawa, T., Motoyoshi, H., Hachikubo, A., Sugiura, K., et al. (2006). In-situ
226 measured spectral directional emissivity of snow and ice in the 8–14 micrometer atmospheric window.
227 *Remote Sensing of Environment* 100, 486 – 502
- 228 Meteoblue (2020). Climate schwarzsee [Available at https://www.meteoblue.com/en/weather/historyclimate/climatemodeled/schwarzsee_switzerland_11790334, accessed 2019-10-01]
- 231 Mölg, T. and Hardy, D. R. (2004). Ablation and associated energy balance of a horizontal glacier surface
232 on kilimanjaro. *J. Geophys. Res.-Atmos.* 109, 1–13. doi:10.1029/2003JD004338
- 233 Oerlemans, J. and Knap, W. H. (1998). A 1 year record of global radiation and albedo in the
234 ablation zone of morteratschgletscher, switzerland. *Journal of Glaciology* 44, 231–238. doi:10.
235 3189/S0022143000002574
- 236 Scherrer, S. C. (2020). Temperature monitoring in mountain regions using reanalyses: lessons from the
237 alps. *Environmental Research Letters* 15, 044005
- 238 Schmidt, L. S., Aðalgeirsþóttir, G., Guðmundsson, S., Langen, P. L., Pálsson, F., Mottram, R., et al. (2017).
239 The importance of accurate glacier albedo for estimates of surface mass balance on vatnajökull: evaluating
240 the surface energy budget in a regional climate model with automatic weather station observations. *The
241 Cryosphere* 11, 1665–1684. doi:10.5194/tc-11-1665-2017
- 242 WMO (2018). *Guide to Instruments and Methods of Observation* (World Meteorological Organization ;
243 2018 (2018 Edition))
- 244 Woolf, H. M. (1968). *On the Computation of Solar Elevation Angles and the determination of sunrise and
245 sunset times* (National Aeronautics and Space Administration)
- 246 Zhou, S., Kang, S., Gao, T., and Zhang, G. (2010). Response of zhadang glacier runoff in nam co basin,
247 tibet, to changes in air temperature and precipitation form. *Chinese Science Bulletin* 55, 2103–2110.
248 doi:10.1007/s11434-010-3290-5